$M1$ decay of the $2\,^3S_1$ state in heliumlike krypton

S. Cheng,* R. W. Dunford, C. J. Liu,† and B. J. Zabransky
Physics Division, Argonne National Laboratory, Argonne, Illinois 60439

A. E. Livingston
Department of Physics, University of Notre Dame, Notre Dame, Indiana 46556

L. J. Curtis
Department of Physics and Astronomy, University of Toledo, Toledo, Ohio 43606
(Received 17 September 1993)

We report a measurement of the lifetime of the $2\,^3S_1$ state in two-electron krypton. The lifetime is found to be 171.0±2.2 ps, which is in reasonable agreement with current theoretical calculations. This measurement provides a test of the order $(Z\alpha)^2$ relativistic corrections to this lifetime.

PACS number(s): 32.70.Fw, 31.30.Jv, 31.10.+z

I. INTRODUCTION

Theoretical and experimental studies of the lifetime of the $1s2s\,^3S_1$ level in heliumlike ions have been important testing grounds for atomic theory. In 1940, Breit and Teller [1] estimated the decay rates for the metastable $2s$ states in H and He. For the $2\,^2S_{1/2}$ level in hydrogen they found that two-photon decay dominated over $M1$ decay in hydrogen, confirming an earlier prediction by Maria Goeppert-Mayer [2,3]. For helium they predicted that the $2\,^1S_0$ level and the $2\,^3S_1$ level also decay predominantly by two-photon emission. However, in 1969, Gabriel and Jordan [4] noticed lines in the soft-x-ray spectrum of the sun corresponding to the $2\,^3S_1 \rightarrow 1\,^1S_0$ transition energies of He-like C V, O VII, Ne IX, Mg XI, and Si XIII. Their observations suggested a significant M1 branch for the decay of the $2\,^3S_1$ level. Griem [5,6] confirmed the interpretation of these lines as single-photon transitions from $2\,^3S_1$, pointing out that Breit and Teller had greatly underestimated the $M1$ decay rate for the $2\,^3S_1$ level. Griem found that the $M1$ decay mode was orders of magnitude greater than the two-photon decay mode for this state. Shortly thereafter, Marrus and Schmieder observed the $M1$ decay of the $2\,^3S_1$ level in beam-foil experiments at Berkeley [7,8].

Subsequent experimental work has resulted in measurements of the $2\,^3S_1$ decay rate ranging from $Z=2$ to $Z=54$. Reviews of results prior to 1978 have been given by Sucher [9] and by Marrus and Mohr [10]. The emphasis recently has been on improved precision at intermediate to high Z in order to test theory in the regime where electron correlations and higher-order relativistic corrections are simultaneously important. In addition to providing a test of theoretical atomic calculations, precise knowledge of the decay rate of the $2\,^3S_1$ state is important in the study of astrophysical and terrestrial plasmas. By comparison of observed and theoretical lifetimes, electron densities in plasmas can be determined [4].

The matrix element for the decay $2\,^3S_1 \rightarrow 1\,^1S_0 + \gamma$ vanishes in a lowest-order calculation using nonrelativistic wave functions, since to first order the operator for magnetic dipole transitions affects only the spin and orbital angular momentum parts of the wave function, and the radial parts are orthogonal. A nonvanishing result requires a relativistic theory, so these transitions are referred to as relativistic $M1$ transitions. For helium and heliumlike ions the calculation is further complicated by the need to account for electron-electron correlations. Following Griem's work, more accurate calculations of the $2\,^3S_1$ decay rate were done by Feinberg and Sucher [11], Drake [12,13], Beigman and Safronova [14], and Kelsey and Sucher [15]. Drake did a variational calculation expressed as a power series in Z^{-1}, including terms up to Z^{-9}. These results provide accurate values to lowest order in αZ. Anderson and Weinhold [16] verified the accuracy of Drake's variational wave functions for Ar^{16+} and concluded that Drake's result was good to better than 0.3%. Feinberg and Sucher obtained an accurate value for helium ($Z=2$) by evaluating the matrix element with a six-parameter Hylleraas wave function. All of these lowest-order calculations are in good agreement with each other.

Higher-order corrections to the $2\,^3S_1$ decay rate have been considered by Lin and Feinberg [17], Kelsey [18,19], Feneuille and Koenig [20], and Johnson and Lin [21]. Radiative, recoil, and retardation effects were found to be unimportant, but higher-order relativistic corrections are important for high-Z ions. Lin [22] calculated the order $(\alpha Z)^2$ relativistic corrections with the result that the lowest-order calculations of the transition rates should be multiplied by the factor

*Present address: Department of Physics and Astronomy, University of Toledo, Toledo, OH 43606.
†Present address: AT&T Bell Laboratories, Middletown, NJ 07748.

$$1+1.07(\alpha Z)^2 \ . \tag{1}$$

Sucher [9] derived an explicit formula for the $M1$ decay rate expected to be accurate to better than 2% in the range $15 \leq Z \leq 40$,

$$A_{2^3S_1} = \frac{2}{3}\frac{\alpha(\alpha Z)^{10}m}{972}[1-4.10/Z+6.7/Z^2 + 1.07(\alpha Z)^2] \ . \tag{2}$$

This formula illustrates the Z^{10} dependence for this forbidden $M1$ transition rate.

The order $(\alpha Z)^2$ relativistic corrections have only recently been observed [23] as experiments have become more precise and improvements in accelerator technology have enabled experiments to be extended to higher Z. The most recent experiments at higher Z [24,25] show a deviation from Eq. (2), which might indicate a need for calculations to higher order than $(\alpha Z)^2$. From an experimental point of view, this possibility can be addressed by determining the Z dependence of any discrepancy between theory and experiment. The goal of the present work was to obtain a more precise value for the $2\,^3S_1$ lifetime at $Z=36$. The most precise result in this region [26] is our earlier measurement is heliumlike Br ($Z=35$), which had an experimental uncertainty of about 3%. The recent addition of an electron-cyclotron-resonance (ECR) source and low-energy linear accelerator to the ATLAS facility at Argonne National Laboratory allowed us to obtain intense krypton beams that provided an opportunity for an improved measurement at $Z=36$. An important component of our Br run was the use of an isotope with nuclear spin that coupled the long-lived $2\,^3P_0$ state to the short-lived $2\,^3P_1$ state [27] resulting in a quenching of this level so that it decayed very near the foil. This greatly simplified the decay curve obtained in that experiment since quenching of the $2\,^3P_0$ level left the $2\,^3S_1$ state as the only long-lived component decaying by single-photon emission. In order to achieve a similar situation for Kr, we used Kr gas enriched in the isotope ^{83}Kr and prepared a beam of ions of this isotope. The low-lying energy levels of heliumlike Kr are shown in Fig. 1. In $^{84}Kr^{34+}$, the $2\,^3P_0$ level feeds the $2\,^3S_1$ level, and because it has a longer lifetime, it complicates the decay scheme. In $^{83}Kr^{34+}$ on the other hand, the $2\,^3P_0$ state decays primarily to the ground state which significantly reduces the feeding of the $2\,^3S_1$ state. Also, the quenched lifetime of the $2\,^3P_0$ state is short enough so that only a small fraction of ions formed in this state contribute to the x-ray signal at the closest foil position used for lifetime data.

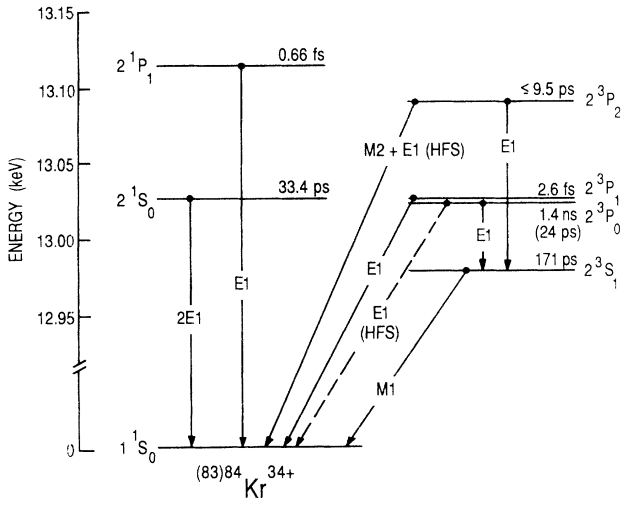

FIG. 1. Low-lying energy levels for heliumlike ^{83}Kr and ^{84}Kr giving the energy levels, lifetimes, and decay modes. Two lifetimes are given for the $2\,^3P_0$ level since this lifetime is different for the two isotopes. The lifetime for this state in ^{83}Kr appears in parentheses. It is reduced by hyperfine quenching which opens up a branch $E1$ (hfs) to the ground state.

II. EXPERIMENT

The krypton ions used in this measurement were extracted from an ECR ion source that was fed with Kr gas enriched in the isotope ^{83}Kr (73 at. %). The beam from the source was mass analyzed and accelerated in ATLAS to a final energy of 639 MeV. The ions then passed through a 200 μg/cm^2 carbon foil where about 12% emerged in the 34+ charge state. These were magnetically selected and directed to our target chamber. The beam velocity was measured to 0.1% using a resonant time-of-flight energy measurement system [28] located between the exit to ATLAS and the 200 μg/cm^2 stripper foil. The energy loss in the stripper foil was determined using a fast Faraday cup located next to the target chamber. By comparing the time of arrival of ions relative to the beam rf reference, with and without the 200 μg/cm^2 stripper foil in place, the energy loss was determined to an accuracy of a few percent. The final correction to the beam velocity measurement was for energy loss in the target foils. This was determined using standard tables for energy loss of ions traversing solids [29].

The apparatus in the target chamber was similar to that used in earlier measurements of forbidden transitions in nickel [30–32] and bromine [26] ions. In the target chamber, the ions passed through a thin carbon foil that was translated along the beam axis. Measurements were made using a number of carbon foils with thicknesses in the range of 20–70 μg/cm^2. Two Si(Li) x-ray detectors located downstream of the foil detected x rays emitted at right angles to the beam. In order to measure the lifetime, the intensity of x rays was measured as a function of the distance from the foil to the region being viewed by the detector. A third, lower resolution, x-ray detector attached to the target stage measured the x-ray intensity at a fixed distance from the foil and provided a normalization. The foil holder was attached to a translation stage whose position was measured by a linear encoder to a precision of 2 μm. One of the detectors was collimated to observe photons in a region 5 mm along the beam, while the other detector was less highly collimated and was used to look for two-photon coincidences.

At each foil position, data were taken for a fixed charge collected at the Faraday cup. Each of the three runs that provided precision lifetime data consisted of three scans over 18 different foil positions. A normaliza-

tion to photons emitted by the beam was obtained from the lower-resolution x-ray detector attached to the foil translation stage. This detector observed a region 10 mm along the beam and provided a check on possible changes in the foil during a measurement. An analysis of the normalization data for each of the three runs showed little change in the normalization count as a function of foil position. This indicates that any changes in foil conditions over the course of a run were adequately averaged by taking multiple scans over the foil positions.

III. RESULTS

Figure 2 is a spectrum from the well-collimated Si(Li) detector width the foil located close to the detector field of view. The intense line near 13 keV is dominated by decays of the $n=2$ levels in heliumlike Kr. The linewidth has contributions from the intrinsic resolution of the detector (200 eV) and the Doppler width due to the finite angular acceptance of the detector. The resolution is not sufficient to resolve the $n=2$ sublevels of heliumlike Kr (see Fig. 1). The broad continuum in the spectrum between 5 keV and 12 keV comes from two-photon decays of the $2\,^1S_0$ level. The blended peaks below 5 keV are transitions into $n=2$ from the $n=3,4,5,\ldots$ levels in two-, three-, and four-electron ions. At each foil position, the $M1$ peak at 13 keV was fitted to a single Gaussian and a linear background to determine the intensity of the line. The intensity as a function of foil position for a typical run is shown in Fig. 3. Several functions were used to fit the decay curves obtained. For each of the three runs, reasonable results were obtained using a fit to a single exponential plus a constant background, but a much better result was obtained from a fit to an exponential plus a power-law term. This function gave excellent fits to all decay curves, and the results for the various data sets gave consistent results for the lifetime. This fitting procedure was justified based on consideration of cascading from higher excited states as discussed below.

A major difficulty in this experiment concerned possible contributions to the line near 13 keV from sources other than $2\,^3S_1$ states created at the foil. Since the various $n=2$ sublevels of $^{83}Kr^{34+}$ are not resolved by our

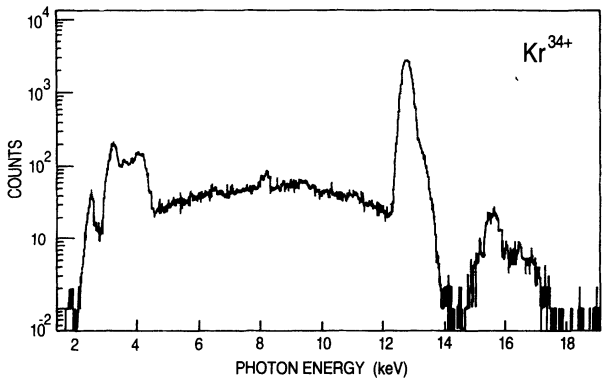

FIG. 2. Typical Si(Li) detector spectrum taken at a small foil-to-detector distance.

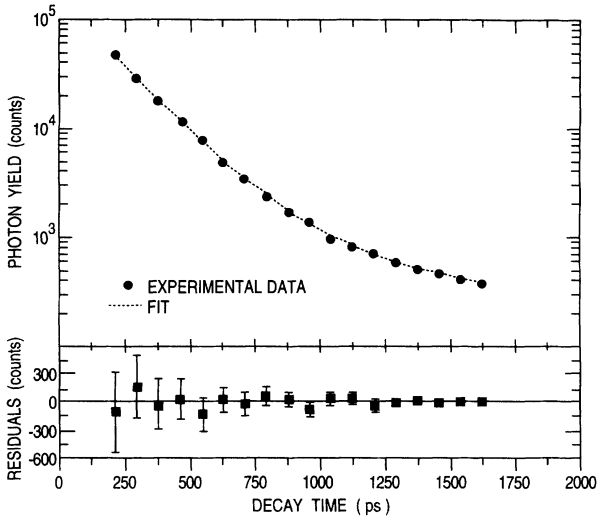

FIG. 3. Intensity decay data for the $M1$ peak. Upper curve is experimental data for one of three runs. The dotted line is a fit to a single exponential plus a power-law background. Lower curve is the residuals from the fit.

Si(Li) detectors, any of these levels could contribute to the peak that we fit to obtain the lifetime. However, at the closest foil position where lifetime data were taken, the $2\,^3S_1$ state is the only $n=2$ state that survives with appreciable probability. The next longest lifetime is that of the $2\,^1S_0$ state which has decayed to less than 0.5% of its initial value before reaching the region being viewed by the detectors. Also, this state does not contribute to the single-photon line since it decays by two-photon emission giving rise to the continuum radiation seen in Fig. 2. As mentioned above, the possible complication from the $2\,^3P_0$ level was eliminated by using the isotope ^{83}Kr, which has a nuclear spin of 9/2. The hyperfine interaction mixes the $2\,^3P_0$ level with the short-lived $2\,^3P_1$ and $2\,^1P_1$ levels. The resulting perturbed $2\,^3P_0$ level has a lifetime of 24 ps [31], so less than 0.05% of the ions formed in this state survive to the field of view of the detectors.

Other contributions to the 13 keV line can arise from cascades through the $2p$ states or from $M1$ decays fed by cascades into $2\,^3S_1$ from higher excited states. The yrast cascades through the $2p$ states give rise to unresolved blends that contribute the largest systematic error to our measurement. An attempt was made to measure the yrast cascades directly by detecting coincidences between the $3d\rightarrow 2p$ transition and the subsequent $2p\rightarrow 1s$ transition. Such coincidences had been observed in our earlier work aimed at studying forbidden transitions in hydrogenlike and heliumlike nickel [30,32]. In the present work we were not able to observe these coincidences because the accidental coincidence rate was too high. The high accidental coincidence rate was caused in part by intense lithiumlike lines that could not be resolved from the heliumlike $3d\rightarrow 2p$ line. After determining that we could not observe the yrast coincidences, we placed 0.007-inch-thick mylar filters on the detectors in order to reduce their rates.

Our method for handling the problem of yrast cascades

in this experiment is based on the fact that their dependence on the foil position is known to fit well to a power law. For example, in our nickel work, an excellent fit to the yrast cascade coincidences was obtained using a power-law function [32]. The power-law form for long-lived yrast cascades was first discussed by Richard [33] and has been established both experimentally [34,35,23] and theoretically [36]. This suggested the fitting function consisting of an exponential plus a power-law term which was used for our final fits to the data.

To estimate the effect of cascades into $2\,^3S_1$ from higher excited states, we measure the transitions $np \rightarrow 1s$ which appear in the Si(Li) spectrum above the 13-keV line. The intensities of these lines can be approximately related to the $np \rightarrow 2s\ 2\,^3S_1$ intensities by considering branching ratios for decay to $1s$ and accounting for singlet-triplet mixing. We assume a statistical distribution over the np sublevels for $n > 2$. Using the derived $np \rightarrow 2s\ 2\,^3S_1$ intensities at each foil position, the rate of repopulation of the $2\,^3S_1$ level as a function of distance downstream of the foil can be estimated [32].

In practice, this procedure was difficult to carry out in the present experiment because of the appearance of peaks in the spectrum above 14 keV arising from the elastic scattering of x rays. The scattering problem is illustrated in Fig. 4, which shows plots of Si(Li) detector spectra from detector 1 at six different foil positions. The foil-to-detector distance increases from the bottom to the top of the figure. Consider the peak on the shoulder of the 13-keV line in the bottom spectrum. As the foil moves farther from the detector, this peak moves toward higher energy. A plot of the energy of the peak as a function of foil position is given in Fig. 5. The schematic diagram in the lower left of the figure suggests an explanation for the origin of the peak. The peak appeared after

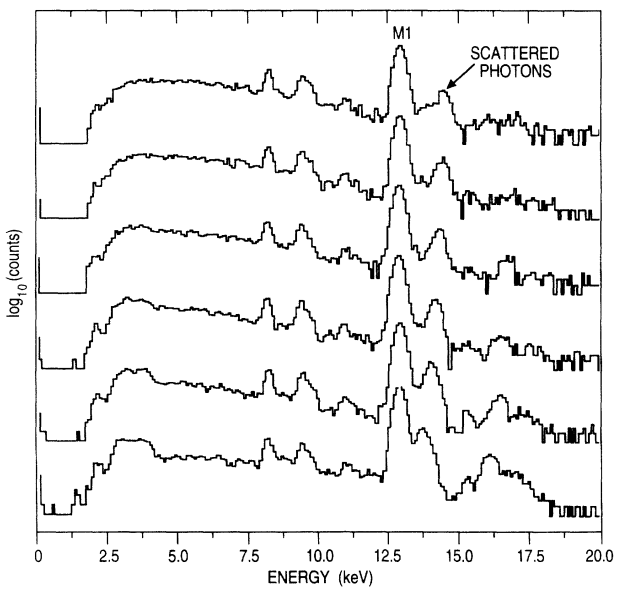

FIG. 4. Si(Li) detector spectra for six foil positions. The peak on the high-energy wing of the $M1$ peak changes position as the foil is moved.

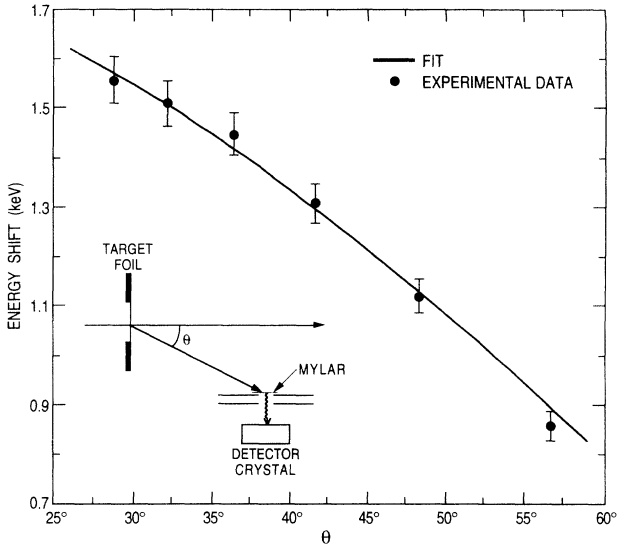

FIG. 5. Energy shift of the elastic scattering peak as a function of the angle between the target foil and the mylar filter. The solid line is a fit of the shift to the Doppler formula.

the mylar filters were placed on the detectors to reduce the intensities of low-energy x rays. Although detector 1 was collimated so that it could not see the flux of x rays coming from the point of interaction of the beam and the foil, these x rays could be scattered by the mylar filter into the detector crystal. Even though the probability of elastic (coherent) scattering of 13-keV photons on mylar is low (about 0.4% [37]), enough photons are produced to form a significant peak in the spectrum. The Doppler shift due to the angle from the beam velocity vector to the detector increases as the foil is moved upstream, shifting the line to higher energy. This Doppler shift is fortunate since the elastic scattered peak is well separated from the $M1$ line. The solid line in Fig. 5 is a fit to the data using the Doppler formula. A good fit is obtained confirming that elastic scattering is the origin of the shifting peaks seen in Fig. 4. Another scattering peak is seen at about 16 keV in the lower spectrum which comes from scattering of x rays from $n=3 \rightarrow n=1$ transitions. In this case, the scattered line is more intense than the $n=3 \rightarrow n=1$ line coming directly from the beam. This observation also fits the scattering model since the intensities of the $n=3 \rightarrow n=1$ transitions drop more rapidly than the intensity of the $M1$ transition as the ions move downstream of the foil. The scattered peaks show a shifted and attenuated version of the spectrum of x rays coming directly from the foil.

Although the scattering peaks are a complication in the determination of the $np \rightarrow 2s$ cascades, a good fit to the region above 14 keV can be performed, and the small correction for these cascades can be determined. As shown in Table I, the $np \rightarrow 2s$ cascades do not contribute significantly to the final error in the measurement.

The results for three separate measurements of the $2\,^3S_1$ lifetime are listed in Table I together with the most important errors and uncertainties. Each measurement consisted of three separate scans of the decay curve. At each foil position data were accumulated for a fixed

TABLE I. Corrections and uncertainties.

Result	Lifetime (ps)
Run 1 fit (21 μg/cm^2 C foil)	172.5±1.6
Run 2 fit (21 μg/cm^2 C foil)	171.6±1.7
Run 3 fit (78 μg/cm^2 C foil)	169.2±1.5
Combined	171.0±0.9
Uncertainty in power-law fit (yrast cascades)	±1.8
Cascades[a] into $2\,^3S_1$	(−0.1±0.6)
H-like $2\,^2S_{1/2}$ $M1$ contribution	±0.1
Velocity measurement error	±0.8
Time dilation[a]	(−1.42)
Final result	171.0±2.2

[a]Corrections and uncertainties in parenthesis were included in the fit result.

amount of charge collected on a Faraday cup located downstream of the target chamber. The three results agree within errors and in particular there is no significant difference between the results from the 21-μg/cm^2 foils and the 78-μg/cm^2 foil. We simply combined the results from the three runs to obtain our final results. The dominant error is the uncertainty in the treatment of the yrast cascades. We also considered possible contributions from Li-like doubly excited states or other multiply excited states but found these effects to be negligible at our present level of precision. X rays from doubly excited states in lithiumlike calcium have been studied at ATLAS in experiments utilizing a high-resolution crystal spectrometer [38].

TABLE II. Theoretical and experimental results for the lifetime of the $2\,^3S_1$ level in heliumlike ions.

			Theory (sec)		
Z	A	Experiments (sec)	Drake[a]	Sucher[b]	Johnson and Lin[c]
2	4	$(9.1+4.0-2.0)\times10^{3}$ [d]	7.864×10^{3}	8.41×10^{3}	7.981×10^{3}
3	6,7	58.6±12.9[e]	49.02		49.09
10	20	$(90.5\pm1.5)\times10^{-6}$ [f]	91.35×10^{-6}		91.07×10^{-6}
16	32	$(706\pm86)\times10^{-9}$ [g]	698.2×10^{-9}	696.4×10^{-9}	698.3×10^{-9}
17	35	$(280\pm25)\times10^{-9}$ [h]	374.0×10^{-9}	373.2×10^{-9}	374.3×10^{-9}
		$(354\pm24)\times10^{-9}$ [g]			
18	40	$(172\pm30)\times10^{-9}$ [i]	207.8×10^{-9}	207.4×10^{-9}	208.0×10^{-9}
		$(172\pm12)\times10^{-9}$ [j]			
		$(202\pm20)\times10^{-9}$ [k]			
		$(203\pm12)\times10^{-9}$ [l]			
22	48	$(25.8\pm1.3)\times10^{-9}$ [j]	26.40×10^{-9}	26.45×10^{-9}	26.55×10^{-9}
23	51	$(16.9\pm0.7)\times10^{-9}$ [m]	16.78×10^{-9}	16.77×10^{-9}	16.84×10^{-9}
26	56	$(4.8\pm0.6)\times10^{-9}$ [m]	4.774×10^{-9}	4.778×10^{-9}	4.798×10^{-9}
35	79	$(224.1\pm7.1)\times10^{-12}$ [n]	226.1×10^{-12}	227.3×10^{-12}	228.2×10^{-12}
36	84	$(200\pm60)\times10^{-12}$ [o]	169.3×10^{-12}	170.2×10^{-12}	171×10^{-12}
	83	$(171.0\pm2.2)\times10^{-12}$ [p]			
41	93	$(45.44\pm0.14)\times10^{-12}$ [q]	44.35×10^{-12}	44.77×10^{-12}	
47	107	$(11.1\pm0.2)\times10^{-12}$ [r]	10.81×10^{-12}	10.96×10^{-12}	
	109	$(11.2\pm0.2)\times10^{-12}$ [r]			
54	132	$(2.554\pm0.076)\times10^{-12}$ [s]	2.555×10^{-12}	2.608×10^{-12}	

[a]Based on the results of Ref. [12] using the energies given in [39] and corrected for nuclear motion [41,40].
[b]Reference [9] corrected for nuclear motion [41,40].
[c]Reference [21] $Z=36$ from Refs. [43,44].
[d]References [45,46]. This uncertainty is 2σ.
[e]Reference [47].
[f]Reference [48].
[g]Reference [49].
[h]Reference [50].
[i]Reference [51].
[j]Reference [52].
[k]Reference [53].
[l]Reference [54].
[m]Reference [55].
[n]Reference [26].
[o]Reference [53].
[p]This work.
[q]Reference [24].
[r]Reference [25].
[s]Reference [23], this paper reports a multiconfiguration Dirac-Fock Coulomb self-consistent value by Indelicato of 2.616 ps.

IV. CONCLUSION

Table II lists all of the experimental results obtained so far together with the results of three theoretical calculations. The column marked "Drake" is based on the formulas from Ref. [12] and energies from Ref. [39]. We also applied the relativistic correction obtained by D. L. Lin [see Eq. (1)]. The column marked "Sucher" is based on his explicit formula [9] [see Eq. (2)], except the result for $n=2$, which is from Ref. [11]. We applied a correction to both the Drake and Sucher results to account for the motion of the nucleus in the center of mass of the ions. This correction was discussed by Bacher [40] and by Fried and Martin [41]. Nuclear motion gives rise to a correction to the effective charge of the electron. Following Drake [42], we define the effective radiative charge of the electron as

$$q_{\text{eff}} = -Z_r e \tag{3}$$

with

$$Z_r = \frac{(Z-n)m}{M+nm} + 1 \ . \tag{4}$$

Here, n is the number of electrons in the ion, m is the electron mass, and M is the nuclear mass. The correction for nuclear motion then involves multiplying the $M1$ transition probabilities by $(Z_r)^2$. Finally, the last column in Table II gives the result of a Dirac-Hartree-Fock calculation by Johnson and Lin [21].

All of the theoretical results in Table II are in substantial agreement, so in Fig. 6 we compare the most precise experimental results with Drake's calculation corrected for relativistic effects and nuclear motion. This is a plot of the difference between theory and experiment expressed as a percentage of the theoretical result. The dotted line gives the change in the theoretical result obtained by leaving out the order $(\alpha Z)^2$ relativistic correction. The six results above $Z=30$ provide good confirmation of this correction. There is generally good agreement between the experimental results and the calculations of Drake and of Sucher except for the most precise experimental result in niobium ($Z=41$). The niobium result suggests a need for inclusion of relativistic corrections beyond $(\alpha Z)^2$. Support for this conclusion comes from the fact that our result at $Z=36$ and the four results at higher Z all give longer lifetimes than theory. Indelicato [23] has performed multiconfigurational Dirac-Fock calculations for $Z=47$ and 54, which agree with experiment.

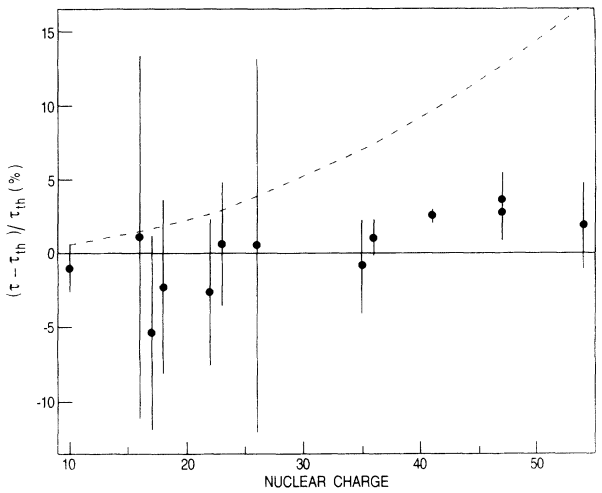

FIG. 6. Comparison of experiment and theory for the lifetime of the $2\,^3S_1$ in helium like ions. The data points are the differences between experiment and theory as a percentage of the theoretical value for the most accurate experiments. The error bars are the experimental errors. We compare to Drake's theoretical values as given in Table II. The theoretical values have been corrected for order $(\alpha Z)^2$ relativistic corrections and for nuclear motion. The broken line indicates the change in theoretical result if the $(\alpha Z)^2$ relativistic correction is left out. References and comparison with other theoretical results are given in Table II.

ACKNOWLEDGMENTS

We are indebted to the ATLAS staff for excellent technical assistance during this experiment. We also thank Elizabeth Vokurka and Heidi Reichenbach who helped with the data analysis. This work was supported by the U.S. Department of Energy, Office of Basic Energy Sciences, under Contract No. W-31-109-ENG-38 (ANL), and Grants No. DE-FG05-88ER13958 (University of Toledo) and No. DE-FG02-92ER14283 (University of Notre Dame).

[1] G. Breit and E. Teller, Astrophys. J. **91**, 215 (1940).
[2] M. Göppert, Naturwiss. **17**, 932 (1929).
[3] M. Goeppert-Mayer, Ann. Phys. (Leipzig) **9**, 273 (1931).
[4] A. H. Gabriel and C. Jordan, Nature (London) **221**, 947 (1969).
[5] H. K. Griem, Astrophys. J. **156**, L103 (1969).
[6] H. K. Griem, Astrophys. J. **161**, L155 (1970).
[7] R. Marrus and R. W. Schmieder, Phys. Lett. **32A**, 431 (1970).
[8] R. W. Schmieder and R. Marrus, Phys. Rev. Lett. **25**, 1245 (1970).
[9] J. Sucher, At. Phys. **5**, 415 (1977).
[10] R. Marrus and P. J. Mohr, Adv. At. Mol. Phys. **14**, 181 (1978).
[11] G. Feinberg and J. Sucher, Phys. Rev. Lett. **26**, 681 (1971).
[12] G. W. F. Drake, Phys. Rev. A **3**, 908 (1971).
[13] G. W. F. Drake, Phys. Rev. A **5**, 1979 (1972).
[14] I. L. Beigman and U. I. Safronova, Zh. Eksp. Teor. Fiz. **60**, 2045 (1971) [Sov. Phys. JETP **33**, 1102 (1971)].
[15] E. J. Kelsey and J. Sucher, Phys. Rev. A **11**, 1829 (1975).
[16] M. T. Anderson and F. Weinhold, Phys. Rev. A **11**, 442 (1975).
[17] D. L. Lin and G. Feinberg, Phys. Rev. A **10**, 1425 (1974).
[18] E. J. Kelsey, Ph.D. thesis, University of Maryland, 1974

(unpublished).
[19] E. J. Kelsey, Ann. Phys. (N.Y.) **98**, 462 (1976).
[20] S. Feneuille and E. Koenig, C. R. Acad. Ser. B **274**, 46 (1972).
[21] W. R. Johnson and C. P. Lin, Phys. Rev. A **9**, 1486 (1974).
[22] D. L. Lin, Ph.D. thesis, Columbia University, 1975 (unpublished).
[23] R. Marrus, P. Charles, P. Indelicato, L. de Billy, C. Tazi, J. P. Briand, A. Simionovici, D. D. Dietrich, F. Bosch, and D. Liesen, Phys. Rev. A **39**, 3725 (1989).
[24] A. Simionovici, B. B. Birkett, P. Charles, D. D. Dietrich, K. Finlayson, P. Indelicato, and R. Marrus, Bull. Am. Phys. Soc. **37**, 1117 (1992).
[25] B. B. Birkett, J. P. Briand, P. Charles, D. D. Dietrich, K. Finlayson, P. Indelicato, D. Liesen, R. Marrus, and A. Simionovici, Phys. Rev. A **47**, 2454 (1993).
[26] R. W. Dunford, D. A. Church, C. J. Liu, H. G. Berry, M. L. A. Raphaelian, M. Hass, and L J. Curtis, Phys. Rev. A **41**, 4109 (1990).
[27] Note that we use *LS* coupling notation in this paper but the states of Br^{33+} and Kr^{34+} are actually closer to *j-j* coupling, so there is also a nonvanishing matrix element of the hyperfine interaction between the $2\,^3P_0$ and $2\,^1P_1$ levels in these ions.
[28] R. Pardo, B. E. Clifft, P. Denhartog, D. Kovar, W. Kutschera, and K. E. Rehm, Nucl. Instrum. Methods **A270**, 226 (1988).
[29] J. F. Ziegler, *Handbook of Stopping Cross Sections for Energetic Ions in all Elements* (Pergamon, New York, 1980).
[30] R. W. Dunford, M. Hass, E. Bakke, H. G. Berry, C. J. Liu, M. L. A. Raphaelian, and L. J. Curtis, Phys. Rev. Lett. **62**, 2809 (1989).
[31] R. W. Dunford, C. J. Liu, J. Last, N. Berrah-Mansour, R. Vondrasek, D. A. Church, and L. J. Curtis, Phys. Rev. A **44**, 764 (1991).
[32] R. W. Dunford, H. G. Berry, D. A. Church, M. Haas, C. J. Liu, M. L. A. Raphaelian, B. J. Zabransky, L. J. Curtis, and A. E. Livingston, Phys. Rev. A **48**, 2729 (1993).
[33] P. Richard, Phys. Lett. **45A**, 13 (1973).
[34] P. Richard, R. L. Kauffman, F. F. Hopkins, C. W. Woods, and K. A. Jamison, Phys. Rev. Lett. **30**, 888 (1973).
[35] W. J. Braithwaite, D. L. Matthews, and C. F. Moore, Phys. Rev. A **11**, 465 (1975).
[36] R. W. Hasse, H. D. Betz, and F. Bell, J. Phys. B **12**, L711 (1979).
[37] E. Storm and H. I. Israel, Nucl. Data Tables **A7**, 565 (1970).
[38] J. Suleiman, H. G. Berry, R. W. Dunford, R. D. Deslattes, and P. Indelicato, Phys. Rev. A **49**, 156 (1994).
[39] G. W. F. Drake, Can. J. Phys. **66**, 586 (1988).
[40] R. Bacher, Z. Phys. A **315**, 135 (1984).
[41] Z. Fried and A. O. Martin, Nuovo Cimento **29**, 574 (1963).
[42] G. W. F. Drake, Phys. Rev. A **34**, 2871 (1986).
[43] W. R. Johnson and C. D. Lin, Phys. Rev. A **14**, 565 (1976).
[44] C. D. Lin, W. R. Johnson, and A. Dalgarno, Phys. Rev. A **15**, 154 (1977).
[45] H. W. Moos and J. R. Woodworth, Phys. Rev. Lett. **30**, 775 (1973).
[46] J. R. Woodworth and H. W. Moos, Phys. Rev. A **12**, 2455 (1975).
[47] R. D. Knight and M. H. Prior, Phys. Rev. A **21**, 179 (1980).
[48] B. J. Wargelin, P. Beiersdorfer, and S. M. Kahn, Phys. Rev. Lett. **71**, 2196 (1993).
[49] J. A. Bednar, C. L. Cocke, B. Curnutte, and R. Randall, Phys. Rev. A **11**, 460 (1975).
[50] C. L. Cocke, B. Curnutte, and R. Randall, Phys. Rev. Lett. **31**, 507 (1973).
[51] R. Marrus and R. W. Schmieder, Phys. Rev. A **5**, 1160 (1972).
[52] H. Gould, R. Marrus, and R. W. Schmieder, Phys. Rev. Lett. **31**, 504 (1973).
[53] H. Gould and R. Marrus, Bull. Am. Phys. Soc. **21**, 84 (1976).
[54] G. Hubricht and E. Träbert, Z. Phys. D **7**, 243 (1987).
[55] H. Gould, R. Marrus, and P. J. Mohr, Phys. Rev. Lett. **33**, 676 (1974).

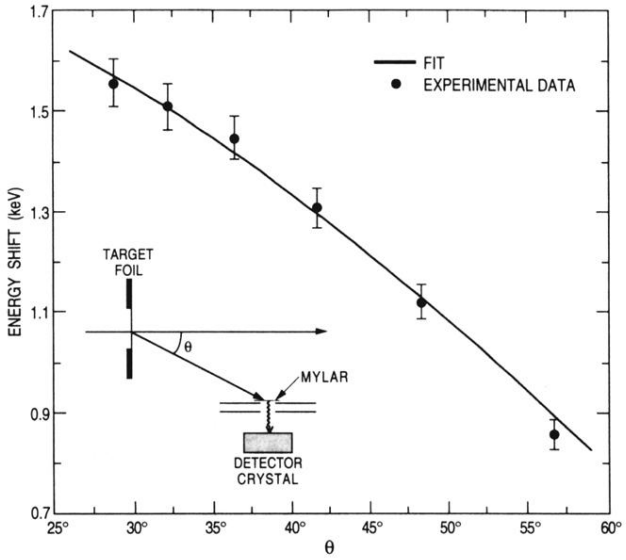

FIG. 5. Energy shift of the elastic scattering peak as a function of the angle between the target foil and the mylar filter. The solid line is a fit of the shift to the Doppler formula.